Polymer 170 (2019) 168–178

Contents lists available at ScienceDirect

Polymer

journal homepage: www.elsevier.com/locate/polymer

Polyaniline-*co*-epichlorohydrin nanoporous anion exchange membranes for diffusion dialysis

Pradeep K. Prajapati[a,b,c], Raghavendra Nimiwal[a], Puyam S. Singh[b,c], Rajaram K. Nagarale[a,c,*]

[a] Electro Membrane Processes Division, CSIR-Central Salt and Marine Chemicals Research Institute (CSIR-CSMCRI), Council of Scientific and Industrial Research (CSIR), GB Marg, Bhavnagar, 364021, India

[b] Membrane Science and Separation Technology Division, CSIR-Central Salt and Marine Chemicals Research Institute (CSIR-CSMCRI), Council of Scientific and Industrial Research (CSIR), GB Marg, Bhavnagar, 364021, India

[c] Academy of Scientific and Innovative Research (AcSIR), CSIR-Central Salt and Marine Chemicals Research Institute (CSIR-CSMCRI), Council of Scientific and Industrial Research (CSIR), GB Marg, Bhavnagar, 364021, India

HIGHLIGHTS

- Convenient and easy synthesis of thermal and chemical stable PANI membranes.
- Highly hydrophilic membranes prepared by double quaternisation.
- High acid recovery of 30–40% from synthetic and effluent solutions at ambient condition.

ARTICLE INFO

Keywords:
Acid recovery
Anion exchange
Diffusion dialysis
Effluent treatment
Polyaniline

ABSTRACT

Nanoporous polyaniline-*co*-epichlorohydrin (PANI-EPH)-based anion exchange membranes on polypropylene substrates were developed by contra-diffusion. Single and double quaternisation were carried out to tune zeta potential, ion-exchange capacity, water contact angle, and percent of water content. Water permeability of 1–1.85 L m^{-2} h^{-1} at 50–200 kPa, and Molecular weight cut-off study indicated the pore size of 4.04–5.85 nm radius. Acid-diffusion study in the static mode led to a proton diffusion coefficient ($U_H{}^+$) of 17×10^{-3} – 20×10^{-3} mh^{-1} and optimum selectivity (S) of 26–32, which were comparable with poly(phenylene oxide), Neosepta, and hydrophilic polyvinyl alcohol (PVA)-based membranes. A very small Fe^{+3} diffusion coefficient ($U_{Fe}{}^{+3}$) of 5×10^{-4} – 7×10^{-4} mh^{-1} was obtained for the synthetic solution by size and charge-dependent exclusion of Fe^{+3} ions (hydrated size of about 0.480 nm) in the nanoporous membranes. For the effluent solution obtained from a local bentonite mine, a $U_H{}^+$ value of 1.5×10^{-3} - 3.5×10^{-3} $mh^{-1}$and $U_{Fe}{}^{+3}$ value of 2.6×10^{-3} - 2.9×10^{-3} mh^{-1} were obtained. These membranes exhibited 33%–40% and 19%–40% acid recovery for synthetic and effluent feed solutions, respectively, suggesting potential utility in acidic effluent treatment.

1. Introduction

Acid recovery from industrial effluents is carried out by diffusion dialysis (DD) using anion-exchange membranes [1,2]. An established technology has been in use worldwide since 1950, when the first industrial plant was demonstrated in Japan [3,4]. The industry reaping the greatest benefits of this technology is the steel processing industry, i.e. pickling spent, where the acid content of the effluent is about 15%–25% and the metal impurity content is 150–250 g/dm^3. Rosacka et al. [5] presented a detailed review on these effluents and their purification. Sulphuric-acid spent is one of the most serious concerns environmentally. Its recovery from diamond manufacturing processes has been demonstrated by Jeong et al. [6] using commercially available anion-exchange membranes. From the initial 4.5 M concentration, 805 g of sulphuric acid could be recovered, i.e. 4.3 M. Poly(2,6-dimethyl-1,4-phenylene oxide) (PPO) and other anion-exchange membranes, both symmetric and asymmetric, for acid recovery from simulated effluent solutions have been reported by Xu's group [7]. The recovery of nickel using an anion-exchange membrane, Neosepta-AFN®, from sulphuric acid containing a Raney Nickel catalyst has been

* Corresponding author. Electro Membrane Processes Division, CSIR-Central Salt and Marine Chemicals Research Institute (CSIR-CSMCRI), Council of Scientific and Industrial Research (CSIR), GB Marg, Bhavnagar, 364021, India.
E-mail address: rknagarale@csmcri.res.in (R.K. Nagarale).

https://doi.org/10.1016/j.polymer.2019.03.016
Received 23 November 2018; Received in revised form 4 March 2019; Accepted 9 March 2019
Available online 13 March 2019
0032-3861/

Abbreviations

DD	Diffusion dialysis
PPO	poly(2,6-dimethyl-1,4-phenylene oxide)
PANI	Polyaniline
PP	Polypropylene
PE	Polyethylene
OPA	Orthophosphoric acid
EPH	Epichlorohydrin
APS	Ammonium persulphate
IPA	Isopropanol
DMF	N,N, dimethylformamide
PVA	Polyvinyl alcohol
TMA	Trimethylamine
PANI-EPH	Polyaniline-*co*-epichlorohydrin
QPANI-EPH	Quaternised polyaniline-*co*-epichlorohydrin
BrQPANI-EPH	Brominated quaternised polyaniline-*co*-epichlorohydrin
IEC	Ion exchange capacity
PEG	Polyethylene glycol
PEO	Polyethyleneoxide
MWCO	Molecular weight cut-off

Symbols

M_C	Mass of coated sample
M_{NC}	Mass of noncoated sample
M_w	Weight of wet sample
M_d	Weight of dry sample
C_f	Concentration of feed
C_p	Concentration of permeate
r_p	Pore radius
S	Separation factor
U	Dialysis coefficient
M	Moles of salute transported per hour
A	Effective area
ΔC	Logarithmic average concentration between two chambers
C_f^0	Feed concentration at initial time
C_f^t	Feed concentration at time, t
C_d^t	Dialysate concentration at time, t
U_{H^+}	Proton diffusion coefficient
$U_{Fe^{+3}}$	Fe^{+3} diffusion coefficient

reported [8]. Reports on polypyrrole-coated Neosepta-AFX® for acid recovery from simulated ferric ion solutions [9] and polysulphone-based anion-exchange membranes are also available [10]. The core polymeric material of these reported anion-exchange membranes are engineering thermoplastics such as PPO, polysulfone, and styrene-divinylbenzene (DVB). Anionic functionalities are usually introduced by chloromethylation in the case of polysulfones and styrene-DVB and bromination in the case of PPO followed by amination. The chloromethylation process uses chloromethyl-methyl-ether as the basic reagent, but it is highly carcinogenic. Herein, we propose an anionic exchanger without chloromethylation using radially available chemicals, such as aniline and epichlorohydrin.

Polyaniline (PANI) has been explored for different applications due to its excellent chemical and thermal stability [11–14]. Its ability for

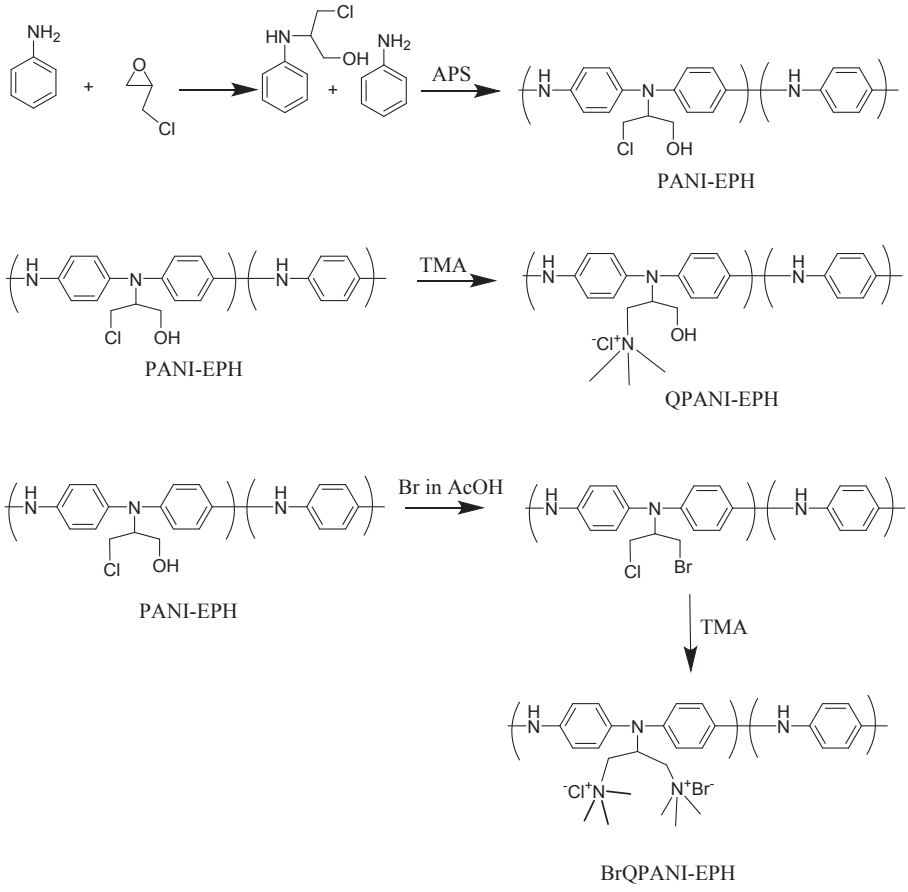

Fig. 1. Schematics of the synthesis of PANI-EPH, QPANI-EPH and BrQPANI-EPH membranes.

proton-coupled anion transport [15] paves the way for utilisation in polyelectrolyte membrane applications. Ruckenstein et al. [16] studied the oxidative coating of conducting polymers on porous polystyrene membranes. Yang et al. [17] reported free-standing conducting films of polypropylene (PP)/PANI by casting solutions of PANI on surfactant-treated PP films. The diffusion of ions through PANI-coated polyethylene (PE) films was reported by Tishchenko et al. [18] Free-standing films were prepared by dipping porous PE films into a solution of aniline hydrochloride and a catalyst. Quiser et al. demonstrated the controlled coating of PANI on hydrophilic cellulose membranes in two-compartment cells [19].

In this study, we report the uniform coating of anion-exchanging PANI film on microporous hydrophobic PP supports by in-situ polymerisation in a two-compartment cell. The prepared membranes were evaluated for their effectiveness in acid separation by diffusion dialysis.

2. Experimental

2.1. Materials

Aniline, epichlorohydrin (EPH), ammonium persulphate (APS), methanol, isopropanol (IPA), and other chemicals were purchased from SD Fine Chemicals, India. Sulphuric acid (H_2SO_4) was obtained from SRL chemicals, India. Trimethylamine (TMA) was procured from Fisher Scientific, India. A 60 μm-thick PP battery separator was purchased from M/s Targray Technology International Inc., Canada. Distilled water was used in all the experiments.

2.2. Synthesis of polyaniline-co-epichlorohydrin based anion exchanger on polypropylene sheets

The synthesis of polyaniline-*co*-epichlorohydrin (PANI-EPH)-based anion exchanger on a hydrophobic PP sheet of 60 μm thickness was carried out by a contra-diffusion process. In brief, 3 mL of aniline and EPH in the ratio of 2:1 were taken in a round-bottomed flask and stirred for 12 h at room temperature (RT). The above solution was slowly mixed with a freshly prepared 3.5 M H_2SO_4 (400 mL) solution. This solution was designated as solution A. Separately, solution B was prepared by the addition of 20 mL of IPA and 4 g of APS in 3.5 M H_2SO_4 (400 mL). Polymerisation was carried out in the contra-diffusion cell in the presence of a PP sheet. Before polymerisation, surface activation of the hydrophobic PP sheet (S-1) was carried out by wetting with IPA. Later, the cell was filled with solution A on one side and solution B on the other side. Both the solutions were recirculated using a peristaltic pump with a flow rate of 24 mL/min for 5 h. After completion of the reaction, the PP sheet was removed from the cell and washed several times with water and stored in water. The obtained membrane was designated as PANI-EPH (S-2). Quaternisation of PANI-EPH on the PP sheet was carried out by dipping the coated PP sheet in 30% TMA for 12 h at RT followed by thorough washing with distilled water. It was designated as QPANI-EPH (S-3). Further, in order to increase the positive character, free −OH groups were converted to methylated bromine and quaternised. This process was carried out by the bromination of PANI-EPH by dipping in 1% bromine in acetic acid for 10 h. Subsequently, the membranes were removed, washed with methanol, and immersed in TMA solution for 12 h for quaternisation, washed, and stored in water. The resulting membrane was designated as BrQPANI-EPH (S-4). A schematic of the reaction steps involved are depicted in Fig. 1.

2.3. Membrane characterisation

The developed membranes were thoroughly characterised for their surface characteristics, hydrophilicity, and water permeability. Contact angle measurement (water) were conducted on a DSA 100 Kruss GmbH instrument at RT. The measurements were carried out at six different locations and the average values were reported. Fourier-Transform Infrared-Attenuated Total Reflectance (FTIR-ATR) spectra were recorded on a Perkin Elmer (Germany) GXFTIR system (with a resolution of ± 4 cm^{-1} and incident angle of 45°) in the wavenumber range of 400–4000 cm^{-1}. Surface morphology was visualised on a JEOL JEM 2100 field-emission scanning electron microscope (FE-SEM) coupled with energy-dispersive X-ray (EDX) spectroscopy at an accelerating voltage of 15–20 kV. Atomic force microscopy (AFM) (Ntegra Aura, NT-MDT, Moscow) was carried out in the semi-contact mode.

Thermogravimetric analysis (TGA, TA Instruments 2960) was performed at a heating rate of 10 °C min^{-1} from RT to 800 °C in N_2 atmosphere. Differential Scanning Calorimetry (DSC) was carried out on a NETZSCH DSC-204F1, Phoenix, instrument at a heating rate of 10 °C min^{-1} from −25 °C to 225 °C at N_2 flow rate of 40 mL/min. The surface charge of the membranes was evaluated by zeta potential (ζ) measurements on a Zeta-CAD, France (version 1.04) instrument using 1 mM KCl as the background electrolyte.

2.3.1. Estimation of the ion-exchange capacity (IEC)

The IEC of the coated membranes was estimated by acid-base titration using a phenolphthalein indicator, as described in previous reports [20,21]. Membranes of known weights were immersed in 0.1 N HCl for 6 h, washed completely with water, and then soaked in 2 N NaCl solution for a minimum of 12 h at RT. Later, the membranes were removed from the NaCl solution and the amount of HCl formed in the NaCl solution (because the process involved ion exchange) was measured by titration against 0.01 N NaOH using a phenolphthalein indicator. The IEC (milli-equivalents of Cl^- per unit dry weight of polymer) was calculated using equation (1).

$$IEC = \frac{NV}{Wdry} \tag{1}$$

Here, N is the normality and V represents the volume of the NaOH solution used. W_{dry} is the dry weight of the membrane in grams.

2.3.2. Coating density and water content measurement

Quantitative estimation of PANI-EPH on the PP sheets was carried out by measuring the coating density (in g/cm^2) using the following equation.

$$Coating\ density\ = \left(\frac{MC - MNC}{MNC}\right) \times 100 \tag{2}$$

M_C is the weight of the coated membrane and M_{NC} is the weight of the non-coated membrane. Membrane samples with an area of 8.55 cm^2 were cut and dried in oven at 60 °C for 20 h prior to weight measurements. The final weight values were taken when a constant weight was attained.

For water content measurements, the membrane samples were cut into spggecific dimensions and immersed in water-filled bottles for 15 h till they reached a constant weight. The samples were taken out from the water, extra surface water was wiped off with Kimwipe tissue paper, and then weighed immediately. The measurements were repeated four times and the average values were used to calculate water content using the following equation,

$$Water\ content\ (\%)\ = \left(\frac{Mw - Md}{Md}\right) \times\ 100 \tag{3}$$

Where M_w is the weight of the wet membrane and M_d is the weight of the dry membrane.

2.3.3. Water flux and molecular-weight cut-off (MWCO) study

Pure water flux of the prepared membranes was measured in the cross-flow mode at an applied pressure of 50–200 kPa using an experimental setup as shown in Fig. 2. The experiments were repeated at least three times to calculate the average water flux. The permeate flux was calculated using the following equation,

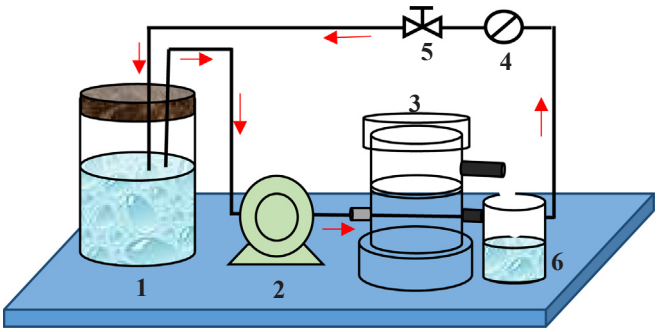

Fig. 2. Schematic of water flux experimental set up; 1) Feed water tank, 2) Booster pump, 3)Testing cell, 4) Pressure gauge, 5) Pressure valve and 6) Permeate collection vessel.

$$J = \frac{V}{At} \tag{4}$$

Where J represents the water flux of the membrane, V is the volume (L) of the permeate, A represents the membrane area (m^2), and t is the time (h) used for the collection of water flux. For determining the MWCO, three solutes, polyethyleneoxide (PEO, Mol. wt. 100 kDa) and polyethyleneglycol (PEG, Mol. wt. 35 kDa and 200 Da) were passed through the membranes at a pressure of 100 kPa. The membrane's MWCO is the molecular weight of those molecules which are retained by 90% from the membrane [22].

The feed and permeate solutions were analysed using gel permeation chromatography (GPC, Waters 2695 Module 2414 RI detector). The concentration of the solutes in the feed and permeate were analysed and the rejection, R(%), of the solute was calculated using the following equation,

$$R(\%) = (1 - \frac{c_p}{c_f}) \times 100 \tag{5}$$

Where, C_f and C_p represents the concentration of the feed and permeate at certain pressure. Using these MWCO values, the pore radius (r_p) of each membrane was calculated using the following equation [23].

$$r_p = \ 0.045 \times MWCO^{0.44} \tag{6}$$

2.3.4. Studies on acid- and iron-diffusion coefficients

Acid diffusion through the membranes was studied using a two-compartment cell. The simulated solution or effluent solution (100 mL) was filled in one compartment while an equal volume of distilled water was filled in the other compartment. The concentration of acid diffused into the water side was measured at every 30 min interval for 6 h. The amount of acid was measured by titration against sodium hydroxide (NaOH) using phenolphthalein indicator. The acid ($U_{H}{}^{+}$) and iron ($U_{Fe}{}^{+3}$) diffusion coefficients were calculated using equation (7) [24].

$$U = \ \frac{M}{At\Delta C} \tag{7}$$

where 'M' is the moles of solute transported per hour, 'A' is an effective membrane area in square meters, 't' is the time in hours, and 'ΔC' is the logarithmic average concentration between the two chambers expressed in moles per cubic metre [19]. It is defined as:

$$\Delta C = \frac{(C_f^0 - C_d^t - C_f^t)}{\ln[(C_f^0 - C_d^t)/C_f^t]} \tag{8}$$

Where, C_f^0 and C_f^t are the feed concentrations at time 0 and t, respectively, and C_d^t is the dialysate concentration at time t. It should be noted that $(C_f^0 - C_d^t - C_f^t)$ is not equal to zero, because water transport through the membrane causes volume changes in the cell chambers during the experiment. The performance of the membranes is determined by the selective diffusion of one species over other present in the solution. It is called the separation factor (S) and is defined as the ratio of the dialysis coefficients (U) of the two species present in the solution (equation (9)).

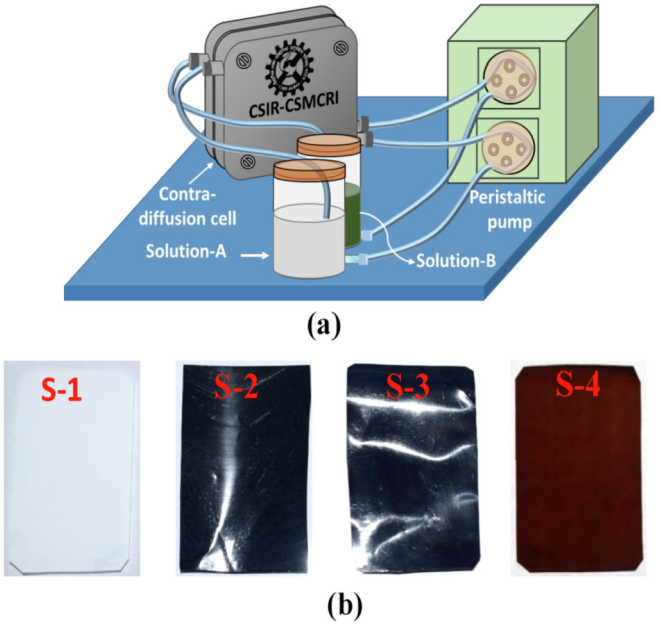

Fig. 3. (a) Schematic of laboratory made two compartment contra-diffusion cell with peristaltic pump and solution reservoirs and (b) photographs of S-1, S-2, S-3 and S-4 membranes.

$$S = \frac{U_{H+}}{U_{Fe+3}} \tag{9}$$

3. Results and discussion

3.1. Membrane synthesis

A PANI-EPH-based anion-exchange material on porous PP sheets was synthesised by the chemical oxidation of aniline and EPH-treated aniline in the presence of sulphuric acid and APS. A schematic of the reaction is presented in Fig. 1. The reaction was carried out in a laboratory-made two-compartment contra-diffusion cell as shown in Fig. 3a. The cell has an effective membrane area of 155.25 cm^2. The solutions in both compartments were allowed to recirculate at a flow rate of 24 mL/min. The progress of the reaction was evident from the changes in the colour of the solution in the diffusion cell. The appearance of a green colour in the aniline-EPH-filled compartment is a clear sign of PANI-EPH formation due to the diffusion of APS through the porous membrane.

It resulted in the formation of PANI-EPH polymer on the aniline side. Fig. 3b shows the images of the coated, quaternised, and brominated quaternised membrane along with the neat PP sheet. Changes in the membrane texture can be clearly visualised. PANI-EPH was dark green in colour and it changed to brown after bromination followed by quaternisation.

3.2. Membrane characterisation

3.2.1. FTIR-ATR spectroscopy

The formation of PANI-EPH was supported by FTIR-ATR spectra in the mid IR region, as shown in Fig. 4. S-1 represents the neat PP sheet. It exhibits strong absorption at ~1377 and 1459 cm^{-1} corresponding to the $-CH_3$ and $-CH_2$ bending of the polymer chain, respectively [17]. In situ polymerisation of PANI-EPH results in new absorption peaks at ~1520 and ~1650 cm^{-1} arising from the N—H deformation of

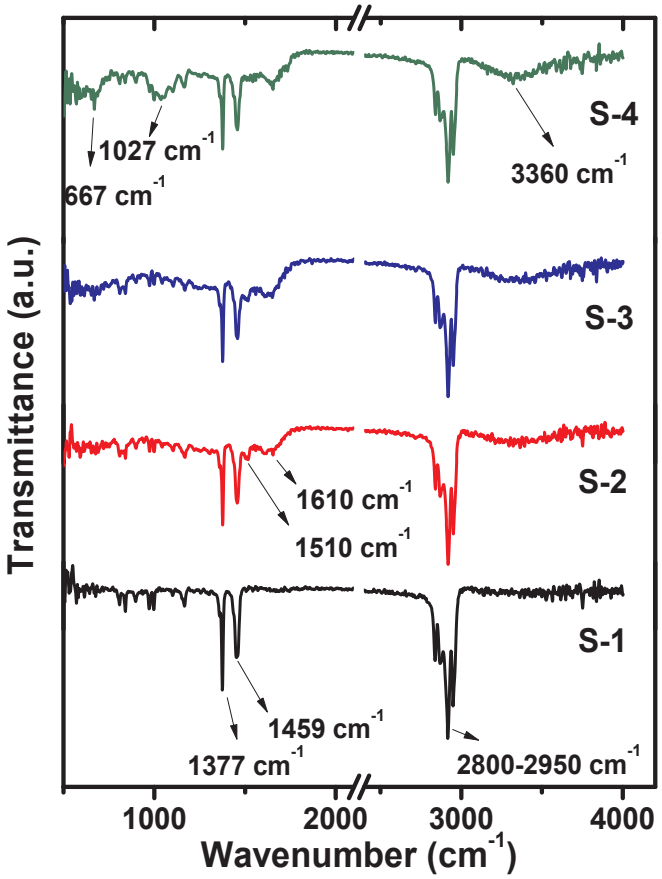

Fig. 4. FTIR -ATR spectra of neat and PANI-EPH membranes (S1, S2, S3 and S4).

secondary amine and C=C stretching of quinoid aromatic rings, respectively [25]. It is accompanied by a strong C–H stretching band at ~2800–2950 cm^{-1} [26]. The broad nature of these peaks indicates an overlap between the N–H bending and C=C stretching bands of aniline. The presence of O–H and N–H stretching is reflected in the broad absorption band at 3300 to 3650 cm^{-1} [27]. Bromination of the membrane results in an additional peak at 667 cm^{-1} corresponding to C–Br stretching. It confirms the successive coating and quaternisation of the membrane.

3.2.2. Coating density, water content, and contact angle measurements

The coating density is a quantitative measurement of the coating efficiency and it was calculated by gravimetric method. The data presented in Table 1 indicates the highest coating density for membrane S-3, followed by membranes S-2 and S-4. The high coating density of S-3 could be attributed to the increase in weight by methylation. Whereas low coating density of S-4 could be attributed to the solubility of some low-molecular weight coated materials during the quaternisation and bromination steps. Partial dissolution is usually observed during the process of IPA washing and bromination in glacial acetic acid; thereafter, the membranes were very stable in the experimental solutions, including the effluent. The lowest coating density observed for membrane S-4 is associated with the partial dissolution of the highly hydrophilic double-quaternised polymer. These observations are reflected in the water content of the membranes; the highest water content of about 79% was observed in S-4. This is followed by membrane S-3 (67% water content) and membrane S-2 (40% water content). Further, these results are supported by the contact angle (θ) measurements.

A contact angle of 0° represents a completely wet surface ($\cos\theta = +1$). On the other hand, a contact angle of 180° represents a completely hydrophobic surface ($\cos\theta = -1$). However, in practice, these values cannot be achieved due to the influence of various external factors on a water drop surface. The data obtained for various membranes are presented in Fig. 5 along with the results of time-dependent measurements. The highest contact angle of > 100° was observed for S-1, i.e. the PP sheet. Upon coating with PANI-EPH, it decreased to ~70° (S-2). Quaternisation results in a further decrease in the contact angle, i.e. to ~60° and ~50° for S-3 and S-4 single and double quaternisation membranes, respectively (Fig. 5A).

The results of the time-dependent measurements of contact angles are presented in Fig. 5B. In the case of S-1, the contact angle remained constant at about ~97° over a period of 6 min. Meanwhile, in the case of S-2, S-3, and S-4, there was a continuous decrease in the contact angle, indicating good surface wettability. This in turn depends on the charge density of the membrane. The lowest contact angle over a 10-min period was observed for S-4 (<30°) double-quaternised membrane, indicating a high charge density. This is followed by S-3 and S-2 membranes with contact angles of <45° and <55°, respectively. The images of time-dependent contact angles over a period of 11 min for membrane S-1, i.e. the neat PP sheet, and S-4, are presented in Fig. 5C for better visualisation. The obtained contact angles for S-2 membrane were comparable to those of neat polyaniline (58° and 53° for doped and undoped polyaniline, respectively) [28].

3.2.3. IEC and zeta potential analysis

IEC is the quantitative measure of ionic groups in the membrane and it is usually determined by acid-base titration and represented in terms of milliequivalents (meq) of ion/g of the dry weight of a membrane. The obtained data for the membranes S-2, S-3, and S-4 are listed in Table 1. As expected, they increased from S-2 to S-4. The membrane S-2 has an IEC of 1.27 meq Cl^-/g, whereas S-3 and S-4 have IEC values of 1.88 and 1.33 meq Cl^-/g, suggesting effective quaternisation of the membranes by bromination followed by treatment with TMA. The IEC of S-4 is lower than S-3 and this may be due to partial dissolution of highly hydrophilic double-quaternised polymer. These values are comparable to the reported values for Nafion [29] and other ion-exchange membranes [30].

The measurement of zeta potential of the membrane surface is a measure of the charged nature of the surface. The obtained values support the IEC and contact-angle measurement results. The measured values are presented in Table 1. Surprisingly, membrane S-1, i.e. neat PP, has a zeta potential of ~ -60 mV. This value is comparable with values reported in the literature [31] with a KCl electrolyte. A high negative zeta potential for neutral PP can be explained on the basis of the accumulation of negative ions in the immobile Stern layers of the electrical double layer [27,32]. The measured zeta potential values for the membranes S-2, S-3, and S-4 were (−32.49 ± 0.97), (−19.66 ± 1.26), and (−6.35 ± 1.03), respectively. These values were less negative than that of neat PP, suggesting partial neutralisation of the accumulated negative charges by the positively charged PANI-co-epichlorohydrin polymer. A low negative value indicates a high positive charge (S-4 > S-3 > S-2). This clearly supports that quaternisation and bromination followed by quaternisation increase the surface charge densities of membranes significantly [27,32,33].

Table 1
Surface charge of the membranes analysed from Zeta potential measurements.

Samples	S-2	S-3	S-4
Zeta potential (mV)	−32.49 ± 0.97	−19.66 ± 1.26	−6.35 ± 1.03
IEC (meq./g)	1.27	1.88	1.33
Water Content (%)	40	67.20	79.89
Coating Density (%)	27.26	31.24	22.39

*Zeta potential value of −60 mV for PP (S-1) support is reported in the literature.

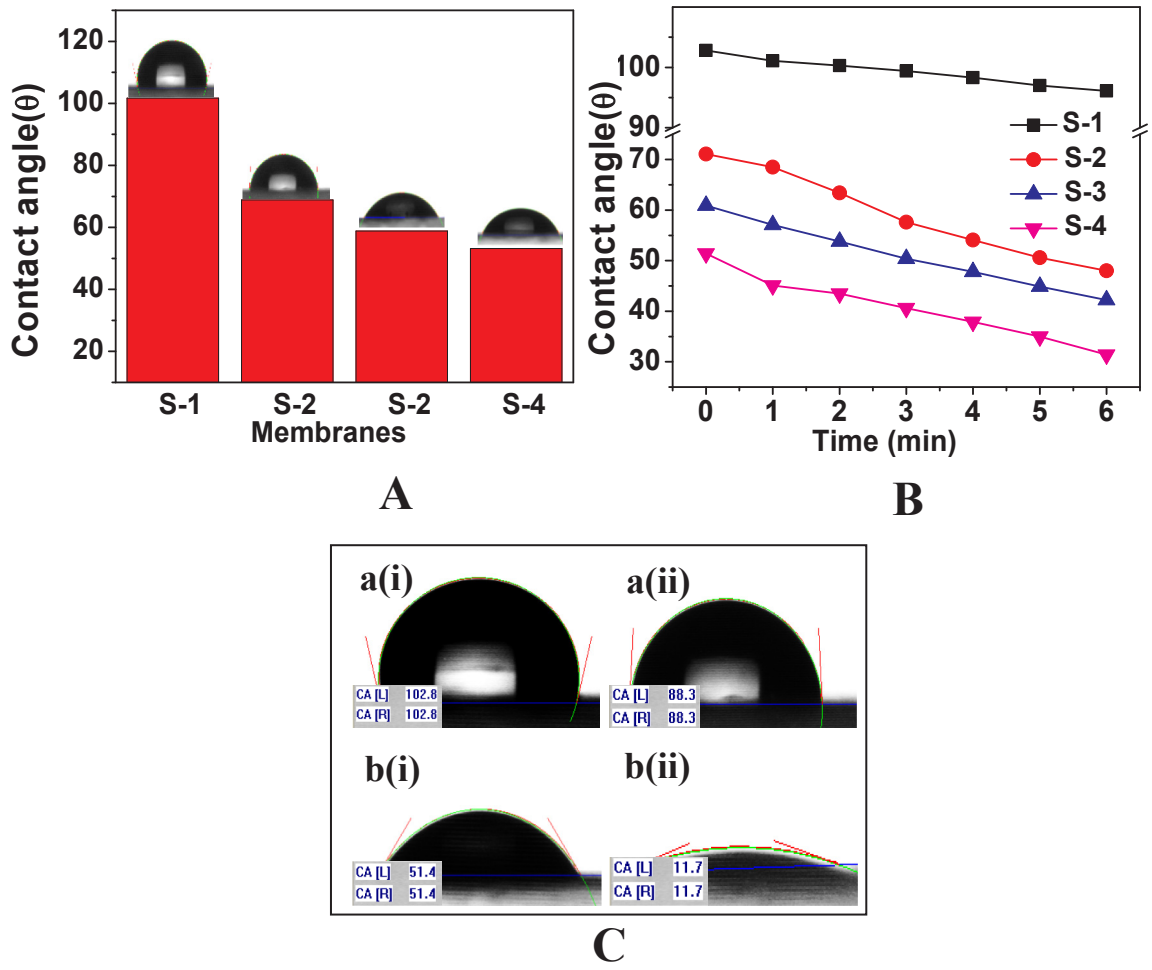

Fig. 5. Contact angle (water) of the membranes; A) at initial time, B) with time variation and C) contact angle images of S1(a) and S4(b) membranes, a(i), b(i) at initial and a(ii), b(ii) after 11 min.

3.2.4. Thermal analysis

The thermal stabilities of all the membranes were evaluated by analysing their DSC and TGA characteristics in an N_2 atmosphere. Fig. 6A shows the recorded DSC thermograms in the temperature range of −20 to 225 °C. The small endothermic peak at ~−15 °C is associated with the free water present in the membrane and it is observed only in coated membranes, i.e. membranes S-2, S-3, and S-4. The melting temperature Fig. 6B shows the results of TGA analysis in an N_2 atmosphere. S-1 membrane exhibited a two-stage decomposition. A very small weight loss occurred at around 300 °C and it is associated with polymer cyclisation. Polymer degradation started at ~350 °C and ended at ~450 °C with more than 90% weight loss. Membrane S-2 also showed a two-step weight loss. The first weight loss stage of ~12% started at ~160 °C, associated with dechlorination and dehydroxylation. Polymer degradation started at ~350 °C and ended at ~450 °C with a comparatively low weight loss or high ash formation than membrane S-1 [34]. Quaternisation of the membranes increased their stability during the first weight loss step by ~2% and 8% for the membranes S-3 and S-4, respectively. Correspondingly, they exhibited high ash formation, indicating an increase in their thermal stability.

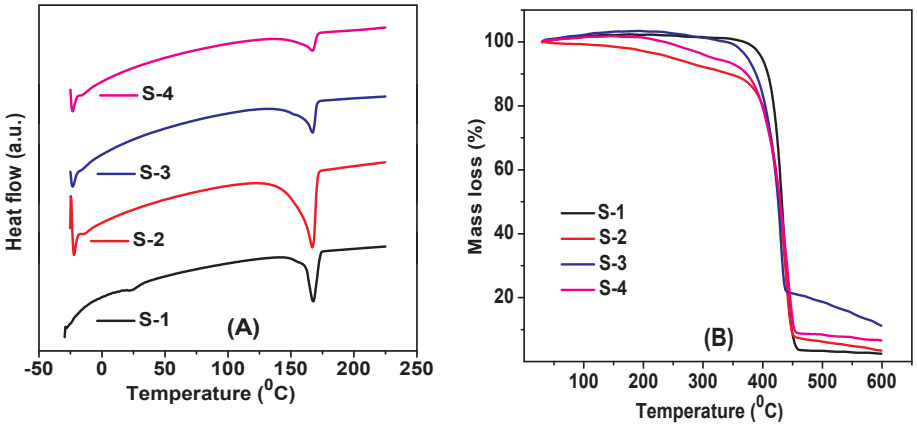

Fig. 6. A) DSC and B) TGA analysis of different membranes in nitrogen atmosphere at heating rate of 10^0/min. of neat PP, membrane S-1, was observed at 169 °C [25]. Membrane S-2 showed a similar melting temperature. However, after quaternisation, membranes S-3 and S-4 showed an increase of about 5 °C in their melting temperatures.

3.2.5. Morphological characterisation

Changes in the surface morphology of the membranes after ANI-EPH polymerisation were evaluated by AFM and SEM imaging. Fig. 7 shows the AFM images of the membranes, along with the neat PP sheet, recorded in the semi-contact mode under ambient conditions on a $10 \times 10\,\mu m^2$ size scale. The phase image shows dark and light shades corresponding to pores and the polymer matrix, respectively. Using these images, we measured the peak-to-peak distances and average roughness values (Table 2). The peak-to-peak distance for the neat PP sheet, i.e. S-1 membrane was ~164.4 nm. After coating with PANI-EPH, it increased to 190.2 n (S-2). In the case of the single and double-

Table 2
Surface roughness parameters and average pore size of the membranes.

Samples	S-1	S-2	S-3	S-4
Peak to Peak (Sy) (nm)	164.4	190.2	249.16	211.38
Mean Value (nm)	68.4	97.7	106.75	97.75
Roughness average(Sa) (nm)	13.3	22.12	17.71	16.41
Root mean square(Sq) (nm)	16.2	27.19	22.20	20.56

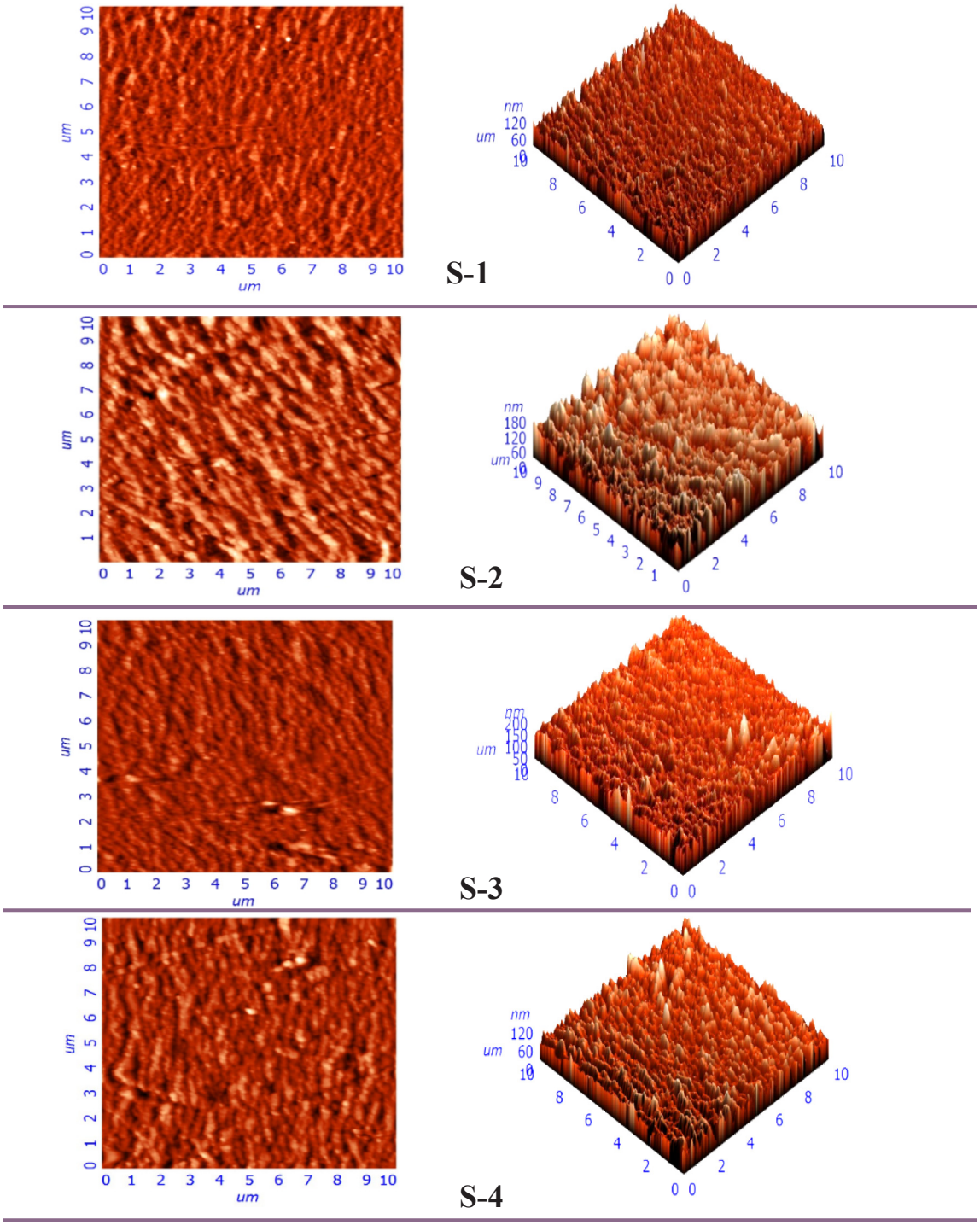

Fig. 7. AFM images of PP support, PANI-EPH, QPANI-EPH and BrQPANI-EPH (S-1, S-2, S-3 and S-4) membranes showing change in surface topology.

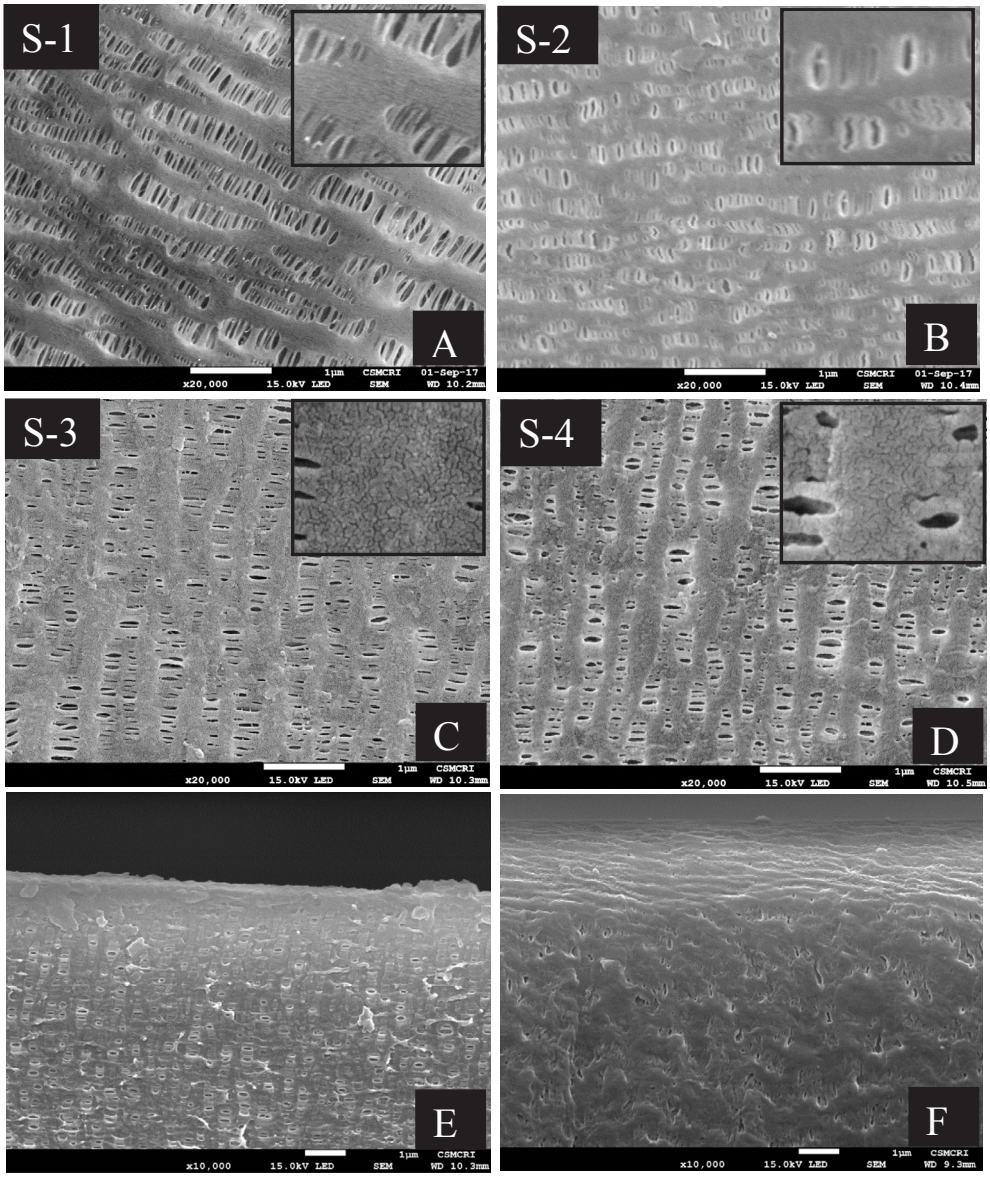

Fig. 8. SEM images showing surface morphologies of S-1(A), S-2(B), S-3(C) and S-4(D) membranes along with magnified images in inset; E) and F) are cross-section images of neat PP sheet (S-1) and BrQPANI-EPH (S-4) membrane respectively.

quaternised membranes S-3 and S-4, the peak-to-peak distances were 249.16 and 211.38 nm, respectively. Fig. 8 shows the SEM images of the coated membranes as well as the neat PP sheet. Fig. 8A suggests a porous structure for the membrane, similar to a typical lithium ion battery separator. It has an average surface pore diameter of about 500 nm. Upon coating with PANI-EPH, the average surface pore width decreased to 50 nm due to the partial filling-in of the membrane pores, as can be clearly observed in Fig. 8B. The coating was uniform without the formation of clusters and/or aggregates (inset of Fig. 8B). After quaterisation, the porosity of the membrane further decreased due to the addition of quaternary ammonium groups in the polymer backbone (membrane S-3, Fig. 8C). The average surface pore width was 300 nm. However, after the addition of a second quaternary group in the polymer backbone by bromination followed by quaternisation, the obtained membrane (membrane S-4, Fig. 8D) exhibited an increase in the membrane pore width. The average surface pore width was 600 nm and this is due to the partial dissolution of the highly hydrophilic polymer by double quaterisation. This is because double quaternisation increases the membrane charge density and water solubility of the polymer. Surface topology images did not yield any insight on the deep penetration of polymers into the pores. SEM cross section images (Fig. 8E and F) were recorded for the synthesised membranes. Fig. 8E represents the neat PP sheet where continuous pores were clearly visible throughout the membrane. Their average pore diameter was similar to the diameter obtained from the surface imaging i.e. ~500 nm. Fig. 8F represents the cross-section image of membrane S-4. From the images it is clear that the pores are not continuous throughout the membranes and their average diameter was far lower than the diameter obtained from surface images. They were in the range of 4–5 nm pore radius obtained from the water permeability experiments. It also gives insight on being surface pore size of about 300–600 nm range and pore radius of 4–5 nm by cross-section, the ions of 0.480 nm can be excluded by the membrane because of its non-continuity of the charged pores. A very uniform coating without aggregation and/or cluster formation is clearly visible in the insets of Fig. 8C and D.

3.2.6. *Studies of water flux and molecular weight cut-off*

In the present study, membranes are prepared by in-situ polymerisation, wherein the polymer gets precipitated deep inside the membrane pores. This phenomenon cannot be properly visualised by

surface characterisation techniques. However, as such penetration affects the water permeability of the membranes, we can deduce the average pore diameter of the membranes from permeability experiments. The experiments were performed at an upstream pressure of 50–200 kPa and the data are presented in Fig. 9. From the Fig., it is clear that neat PP, i.e. membrane S-1, did not show a water flux due to its hydrophobic nature. However, membranes S-2, S-3, and S-4 showed 1–1.85 LMH water flux at 50–200 kPa, indicating a good hydrophilic nature (Fig. 9A). The porosity of the membranes was calculated from the MWCO study. It is a common practice to calculate the pore size of membranes using solutes of different molecular weights, which are passed through the membranes. We performed experiments with 500 ppm solutions of PEG (Mw. 200 Da) and PEG (Mw. 35 kDa) and a 300 ppm solution of PEO (Mw. 100 kDa) at pressures of 50–200 kPa. The percent retention results are presented in Table 3.

From the results, it is clear that the low-molecular weight solute, i.e. PEG (Mw. 200), has low rejection. The obtained values were 41.43%, 54.5%, and 39.5% for membranes S-2, S-3, and S-4, respectively. The highest rejections of 100% and > 98% were observed for PEO (Mw. 100 kDa) and PEG (35 kDa), respectively, with all types of membranes (Fig. 9B). This indicates the dense nature of the membrane after coating. From the Fig., it can be observed that there is a linear correlation between rejection and MWCO values. The obtained MWCO values were 63.3, 27.6, and 29.93 kDa for membranes S-2, S-3, and S-4, respectively. From these values, the pore radius (r_p) of the coated membranes was calculated using equation (6) and the results are presented in Table 3.

The average pore radii of the membranes S-2, S-3, and S-4 were 5.58, 4.04, and 4.20 nm, respectively. These are 100 times lower than the average surface pore diameters obtained from SEM and AFM results, indicating a deep penetration of the polymer into the pores of the membranes, thus transforming them into nanoporous membranes. These types of membranes have been studied for the separation of Fe^{+3} ions [35], which have a hydrated radius of 0.480 nm [36,37] indicating suitability of the synthesised membranes for diffusion dialysis.

3.3. Acid and iron diffusion study

Diffusion dialysis experiments were performed with a synthetic solution as well as the effluent obtained from a local bentonite mine in a two-compartment cell, as shown in Fig. 3A. Initial experiments were carried out with known concentrations of HCl circulating in the left compartment and distilled water in the right compartment. The decrease in acid concentration on the left side and increase in acid concentration on the right side were measured by acid-base titration. The data are presented in Fig. 10A in terms of the percentage of acid recovery with respect to the initial concentration. The initial concentration was kept constant at about 3.5 M. From Fig. 10A, it is clear that in a 6-h experiment, for all the tested membranes, a linear increase in the acid concentration on the right-side compartment was observed. The maximum acid recovery of 40% was obtained for membrane S-4, whereas membranes S-2 and S-3 exhibited an acid recovery of 33%. The higher acid recovery of membrane S-4 is due to its high charge density. When experiments were performed with a synthetic feed, i.e. a solution of 5% $FeCl_3$ in 3.5 M HCl, the maximum acid recovery of 38% was obtained with membrane S-4. The acid recovery values for membranes S-2 and S-3 remained constant at 33%. The results are shown in Fig. 10B. The results of the acid recovery experiments on the effluent obtained from the bentonite mine are presented in Fig. 10C. The best results were obtained with membranes S-3 and S-4 (37% and 40% acid recovery, respectively). Membrane S-2 exhibited a poor acid recovery

Table 3
Pore radius of different PANI membranes.

Membrane	$R(\%)_{PEO\ (100kDa)}$	$R(\%)_{PEG\ (35kDa)}$	$R(\%)_{PEG(200Da)}$	r_p (nm)
S-2	100	98.1	41.43	5.58
S-3	100	99.4	54.5	4.04
S-4	100	98.32	39.56	4.20

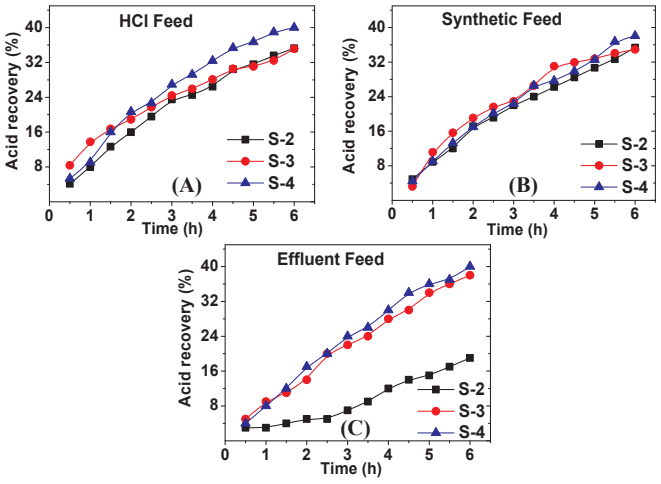

Fig. 10. Acid diffusion study from (A) HCl feed (B) Synthetic feed and (C) effluent feed using the S-2, S-3 and S-4 membranes.

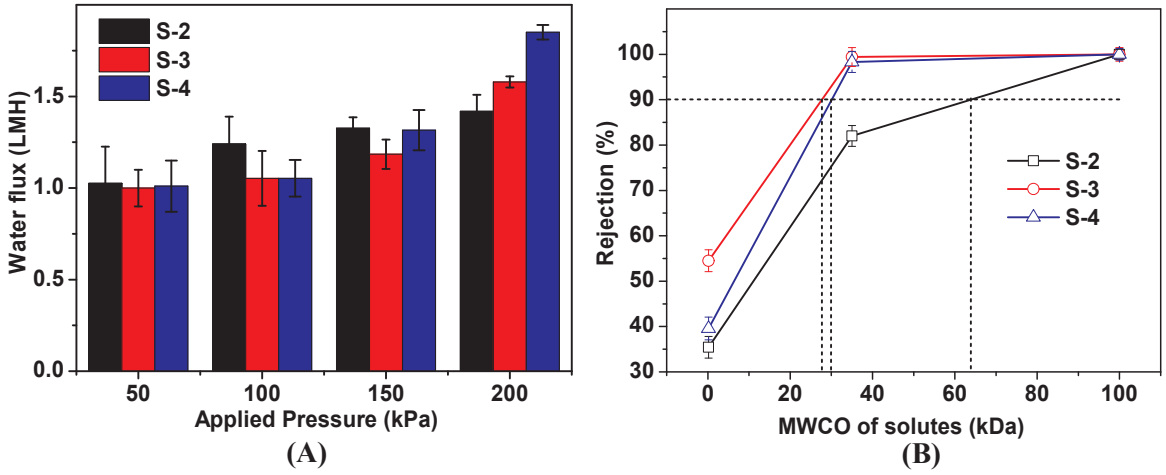

Fig. 9. (A) Pure water flux study at 50–200 kPa and (B) Molecular Weight Cut-off study of S-2, S-3 and S-4 membranes using low to high molecular weight solutes (0.2, 35 and 100 kDa) at applied pressure of 100 kPa.

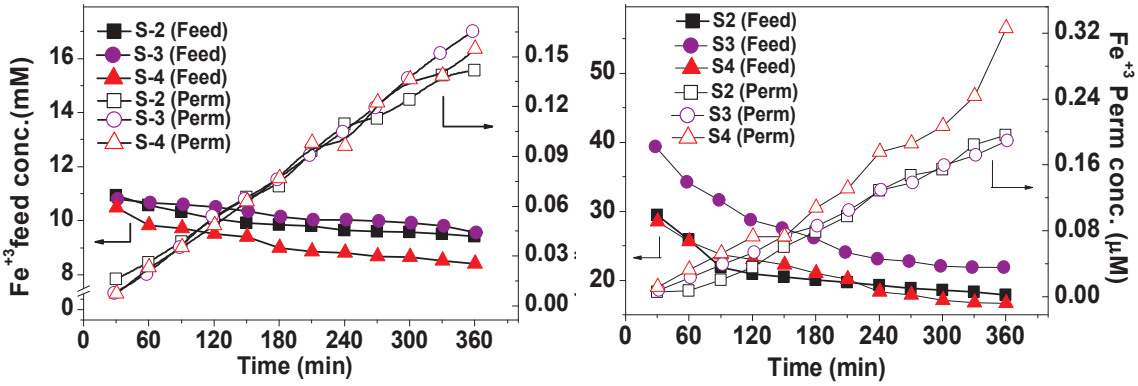

Fig. 11. Fe^{+3} diffusion study with S-2, S-3 and S-4 membranes from (a) synthetic and (b) effluent feed solutions.

of 19%.

Fig. 11 shows the permeability of Fe^{+3} ions in different membranes in synthetic and effluent solutions. From the data, it is clear that very small amounts of Fe^{+3} permeated through the membranes. The lowest permeability was obtained for membrane S-3, followed by S-2 and S-4, suggesting a combined effect of pore diameter and charge density in reducing Fe^{+3} permeation. The calculated diffusion coefficients and separation factors are presented in Fig. 12(a–d). From Fig. 12a, it is clear that the proton diffusion coefficient ($U_H{}^+$) is higher than the Fe^{+3} diffusion coefficient ($U_{Fe}{}^{+3}$). In the synthetic solution, the $U_H{}^+$ values for membrane S-2, S-3, and S-4 were 17×10^{-3}, 21×10^{-3}, and 20×10^{-3}, whereas the $U_{Fe}{}^{+3}$ values were 5×10^{-4}, 7×10^{-4}, and 6×10^{-4} m h^{-1}, respectively. The calculated separation factors are presented in Fig. 12c. The best selectivity of 32 was obtained with membrane S-4. Fig. 12b shows the $U_H{}^+$ and $U_{Fe}{}^{+3}$ data for the effluent solution obtained from the bentonite mine. Membrane S-2 exhibited the best performance. The obtained $U_H{}^+$ and $U_{Fe}{}^{+3}$ values were 1.5×10^{-3}, 3.0×10^{-3}, and 3.5×10^{-3} and 31×10^{-4}, 26×10^{-4}, and 29×10^{-4} m h^{-1}, for S-2, S-3, and S-4, respectively (Fig. 12d). The high permeability of Fe^{+3} ions through the S-2 membrane is due to its poor charged nature compared to S-3 and S-4. But is similar to the reported values [24,38–47] presented in Fig. 13 indicating potential

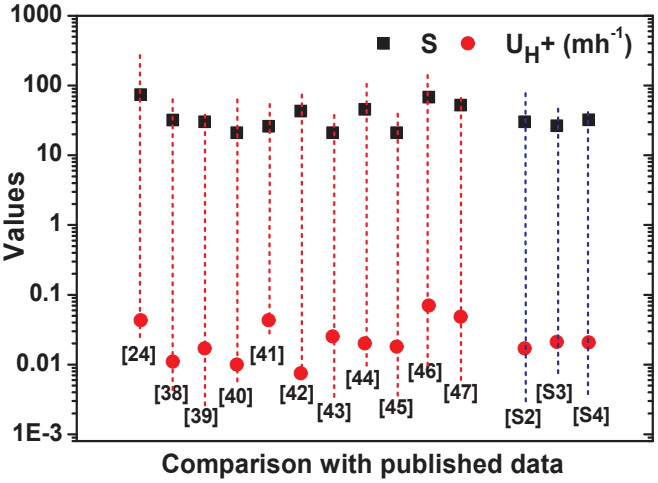

Fig. 13. The published data of diffusion coefficient ($U_H{}^+$) and selectivity (S) of related references in comparison with present study.

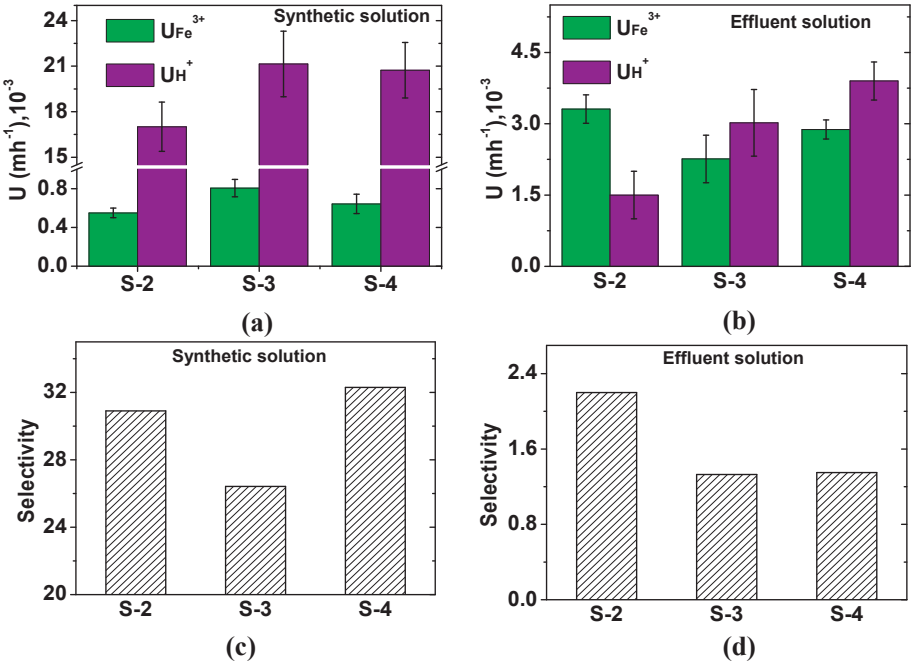

Fig. 12. The study of $U_H{}^+$ and $U_{Fe}{}^{+3}$ diffusion coefficients (a, b) and their selectivity (S) (c, d) by using S-2, S-3 and S-4 membranes from the synthetic and effluent solution respectively.

applications of developed membranes for acid recovery from the effluents.

4. Conclusions

We successfully prepared nanoporous polyaniline-*co*-epichlorohydrin anion-exchange membranes on PP substrates by contra-diffusion and used them for acid separation in synthetic and locally sourced acid effluents from bentonite mines. Physicochemical characterisation revealed the formation of charged nanoporous membranes with 4–5 nm pore radius. In diffusion dialysis experiments, the observed H^+ diffusion coefficient was comparable with the values reported in literature, indicating the potential applicability of these membranes in effluent treatment. Among the prepared membranes (S-2, S-3, and S-4), the highest acid recovery of 40% was observed for membrane S-4 with ${U_H}^+$ and ${U_{Fe}}^{+3}$ values of 20×10^{-3} m h^{-1} and 6×10^{-4} m h^{-1}, respectively. In acid recovery experiments with the bentonite-mine effluent, the highest obtained ${U_H}^+$ and ${U_{Fe}}^{+3}$ values were 3.5×10^{-3} m h^{-1} and 2.9×10^{-3} m h^{-1}, respectively.

Acknowledgements

Director CSIR-CSMCRI is acknowledged for continuous support and encouragement. Instrumentation facility provided by Analytical Discipline & Centralized Instrument Facility, CSIR-CSMCRI, Bhavnagar, are gratefully acknowledged. RKN thanks for the financial support (grant number EMR/2016/00l977) from Science and Engineering Research Board, DST India. PP thanks for the senior research fellowship (SRF) from CSIR, India. CSIR-CSMCRI manuscript number– 072/2018.

References

[1] Y. Nleya, G.S. Simate, S. Ndlovu, Sustainability assessment of the recovery and utilisation of acid from acid mine drainage, J. Clean. Prod. 113 (2016) 17–27.
[2] M. Gernon, Environmental benefits of methanesulfonic acid. Comparative properties and advantages, Green Chem. 1 (1999) 127–140.
[3] S. Tokyyama, Novel anion-exchange membrane, Japan patent EP0375096, (1990).
[4] J. Luo, C. Wu, T. Xu, Y. Wu, Diffusion dialysis-concept, principle and applications, J. Membr. Sci. 366 (2011) 1–16.
[5] M. Regel-Rosocka, A review on methods of regeneration of spent pickling solutions from steel processing, J. Hazard Mater. 177 (2010) 57–69.
[6] J. Jeong, M.-S. Kim, B.-S. Kim, S.-K. Kim, W.-B. Kim, J.-C. Lee, Recovery of H2SO4 from waste acid solution by a diffusion dialysis method, J. Hazard Mater. 124 (2005) 230–235.
[7] L. Ge, A.N. Mondal, X. Liu, B. Wu, D. Yu, Q. Li, J. Miao, Q. Ge, T. Xu, Advanced charged porous membranes with ultrahigh selectivity and permeability for acid recovery, J. Membr. Sci. 536 (2017) 11–18.
[8] H. Bendova, T. Weidlich, Application of diffusion dialysis in hydrometallurgical separation of nickel from spent Raney Ni catalyst, Separ. Sci. Technol. (2017) 1–5.
[9] D.-H. Kim, H.-S. Park, S.-J. Seo, J.-S. Park, S.-H. Moon, Y.-W. Choi, Y.S. Jiong, D.H. Kim, M.-S. Kang, Facile surface modification of anion-exchange membranes for improvement of diffusion dialysis performance, J. Colloid Interface Sci. 416 (2014) 19–24.
[10] M. Ersoz, I. Gugul, A. Sahin, Transport of acids through polyether–sulfone anion-exchange membrane, J. Colloid Interface Sci. 237 (2001) 130–135.
[11] H.D. Tran, J.M. D'Arcy, Y. Wang, P.J. Beltramo, V.A. Strong, R.B. Kaner, The oxidation of aniline to produce "polyaniline": a process yielding many different nanoscale structures, J. Mater. Chem. 21 (2011) 3534–3550.
[12] B. Wang, X. Liu, Q. Liu, J. Chen, H. Jiang, Y. Wang, K. Liu, M. Li, D. Wang, Three-dimensional non-woven poly(vinyl alcohol-co-ethylene) nanofiber based polyaniline flexible electrode for high performance supercapacitor, J. Alloy. Comp. 715 (2017) 137–145.
[13] K. Uh, B. Yoon, C.W. Lee, J.-M. Kim, An electrolyte-free conducting polymer actuator that displays electrothermal bending and flapping wing motions under a magnetic field, ACS Appl. Mater. Interfaces 8 (2016) 1289–1296.
[14] S. Hosseini, F. Jeddi, M. Nemati, S. Madaeni, A. Moghadassi, Electrodialysis heterogeneous anion exchange membrane modified by PANI/MWCNT composite nanoparticles: preparation, characterization and ionic transport property in desalination, Desalination 341 (2014) 107–114.
[15] L. Wen, N. Kocherginsky, Coupled H+/anion transport through polyaniline membranes, J. Membr. Sci. 167 (2000) 135–146.
[16] E. Ruckenstein, J.S. Park, Polythiophene and polythiophene-based conducting composites, Synth. Met. 44 (1991) 293–306.
[17] J. Yang, J. Hou, W. Zhu, M. Xu, M. Wan, Substituted polyaniline-polypropylene film composites: preparation and properties, Synth. Met. 80 (1996) 283–289.
[18] G. Tishchenko, J. Dybal, J. Stejskal, V. Kůdela, M. Bleha, E.Y. Rosova, G. Elyashevich, Electrical resistance and diffusion permeability of microporous polyethylene membranes modified with polypyrrole and polyaniline in solutions of electrolytes, J. Membr. Sci. 196 (2002) 279–287.
[19] A.A. Qaiser, M.M. Hyland, D.A. Patterson, Control of polyaniline deposition on microporous cellulose ester membranes by in situ chemical polymerization, J. Phys. Chem. B 113 (2009) 14986–14993.
[20] C. Steffens, F. Leite, A. Manzoli, R. Sandoval, O. Fatibello, P. Herrmann, Microcantilever sensors coated with doped polyaniline for the detection of water vapor, Scanning 36 (2014) 311–316.
[21] V.K. Sachan, A. Devi, R.S. Katiyar, R.K. Nagarale, P.K. Bhattacharya, Proton transport properties of sulphanilic acid tethered poly(methyl vinyl ether-alt-maleic anhydride)-PVA blend membranes, Eur. Polym. J. 56 (2014) 45–58.
[22] W. Koros, Y. Ma, T. Shimidzu, Terminology for membranes and membrane processes (IUPAC Recommendations 1996), Pure Appl. Chem. 68 (1996) 1479–1489.
[23] J. Mulder, Basic Principles of Membrane Technology, Springer Science & Business Media, 2012.
[24] X. Lin, E. Shamsaei, B. Kong, J.Z. Liu, T. Xu, H. Wang, Fabrication of asymmetrical diffusion dialysis membranes for rapid acid recovery with high purity, J. Mater. Chem. A 3 (2015) 24000–24007.
[25] S. Cho, M. Kim, J.S. Lee, J. Jang, Polypropylene/polyaniline nanofiber/reduced graphene oxide nanocomposite with enhanced electrical, dielectric, and ferroelectric properties for a high energy density capacitor, ACS Appl. Mater. Interfaces 7 (2015) 22301–22314.
[26] B. Han, J. Pan, S. Yang, M. Zhou, J. Li, A. Sotto Diaz, B. Van der Bruggen, C. Gao, J. Shen, Novel composite anion exchange membranes based on quaternized polyepichlorohydrin for electromembrane application, Ind. Eng. Chem. Res. 55 (2016) 7171–7178.
[27] M.C. Lukowiak, S. Wettmarshausen, G. Hidde, P. Landsberger, V. Boenke, K. Rodenacker, U. Braun, J.F. Friedrich, A.A. Gorbushina, R. Haag, Polyglycerol coated polypropylene surfaces for protein and bacteria resistance, Polym. Chem. 6 (2015) 1350–1359.
[28] R. Nagarale, G. Gohil, V.K. Shahi, Recent developments on ion-exchange membranes and electro-membrane processes, Adv. Colloid Interface Sci. 119 (2006) 97–130.
[29] D.M. Stachera, R.F. Childs, A.M. Mika, J.M. Dickson, Acid recovery using diffusion dialysis with poly (4-vinylpyridine)-filled microporous membranes, J. Membr. Sci. 148 (1998) 119–127.
[30] P. Sridhar, G. Subramaniam, Recovery of acid from cation exchange resin regeneration waste by diffusion dialysis, J. Membr. Sci. 45 (1989) 273–280.
[31] P. Slepička, A. Vasina, Z. Kolská, T. Luxbacher, P. Malinský, A. Macková, V. Švorčík, Argon plasma irradiation of polypropylene, Nucl. Instrum. Methods Phys. Res. Sect. B Beam Interact. Mater. Atoms 268 (2010) 2111–2114.
[32] L.S. McCarty, G.M. Whitesides, Electrostatic charging due to separation of ions at interfaces: contact electrification of ionic electrets, Angew. Chem. Int. Ed. 47 (2008) 2188–2207.
[33] R. Zimmermann, S. Dukhin, C. Werner, Electrokinetic measurements reveal interfacial charge at polymer films caused by simple electrolyte ions, J. Phys. Chem. B 105 (2001) 8544–8549.
[34] S. Wang, J. Shang, Q. Wang, W. Zhang, X. Wu, J. Chen, W. Zhang, S. Qiu, Y. Wang, X. Wang, Enhanced electrochemical performance by strongly anchoring highly crystalline polyaniline on multiwalled carbon nanotubes, ACS Appl. Mater. Interfaces 9 (2017) 43939–43949.
[35] B. Ericsson, M. Hallberg, J. Wachenfeldt, Nanofiltration of highly colored raw water for drinking water production, Desalination 108 (1997) 129–141.
[36] B. Tansel, Significance of thermodynamic and physical characteristics on permeation of ions during membrane separation: hydrated radius, hydration free energy and viscous effects, Separ. Purif. Technol. 86 (2012) 119–126.
[37] H. Ohtaki, T. Radnai, Structure and dynamics of hydrated ions, Chem. Rev. 93 (1993) 1157–1204.
[38] J. Luo, C. Wu, Y. Wu, T. Xu, Diffusion dialysis of hydrochloride acid at different temperatures using PPO–SiO2 hybrid anion exchange membranes, J. Membr. Sci. 347 (2010) 240–249.
[39] C. Wu, Y. Wu, J. Luo, T. Xu, Y. Fu, Anion exchange hybrid membranes from PVA and multi-alkoxy silicon copolymer tailored for diffusion dialysis process, J. Membr. Sci. 356 (2010) 96–104.
[40] Y. Wu, C. Wu, Y. Li, T. Xu, Y. Fu, PVA–silica anion-exchange hybrid membranes prepared through a copolymer crosslinking agent, J. Membr. Sci. 350 (2010) 322–332.
[41] Y. Wu, J. Luo, L. Yao, C. Wu, F. Mao, T. Xu, PVA/SiO2 anion exchange hybrid membranes from multisilicon copolymers with two types of molecular weights, J. Membr. Sci. 399 (2012) 16–27.
[42] Y. Wu, J. Luo, C. Wu, T. Xu, Y. Fu, Bionic multisilicon copolymers used as novel cross-linking agents for preparing anion exchange hybrid membranes, J. Phys. Chem. B 115 (2011) 6474–6483.
[43] A.N. Mondal, C. Cheng, Z. Yao, J. Pan, M.M. Hossain, M.I. Khan, Z. Yang, L. Wu, T. Xu, Novel quaternized aromatic amine based hybrid PVA membranes for acid recovery, J. Membr. Sci. 490 (2015) 29–37.
[44] F. Sun, C. Wu, Y. Wu, T. Xu, Porous BPPO-based membranes modified by multisilicon copolymer for application in diffusion dialysis, J. Membr. Sci. 450 (2014) 103–110.
[45] C. Cheng, Z. Yang, J. Pan, B. Tong, T. Xu, Facile and cost effective PVA based hybrid membrane fabrication for acid recovery, Separ. Purif. Technol. 136 (2014) 250–257.
[46] J. Pan, Y. He, L. Wu, C. Jiang, B. Wu, A.N. Mondal, C. Cheng, T. Xu, Anion exchange membranes from hot-pressed electrospun QPPO–SiO2 hybrid nanofibers for acid recovery, J. Membr. Sci. 480 (2015) 115–121.
[47] K. Emmanuel, C. Cheng, B. Erigene, A.N. Mondal, M.M. Hossain, M.I. Khan, N.U. Afsar, G. Liang, L. Wu, T. Xu, Imidazolium functionalized anion exchange membrane blended with PVA for acid recovery via diffusion dialysis process, J. Membr. Sci. 497 (2016) 209–215.